Mon. Not. R. Astron. Soc. **000**, 1–10 (2015) Printed 12 May 2016 (MN LATEX style file v2.2)

A spectroscopic study of the Globular Cluster NGC 4147

S. Villanova[1⋆], L. Monaco[2], C. Moni Bidin[3], and P. Assmann[4,5,1]
[1] *Departamento de Astronomia, Casilla 160, Universidad de Concepción, Chile*
[2] *Universidad Andres Bello, Departamento de Ciencias Fisicas, Republica 220, Santiago, Chile*
[3] *Instituto de Astronomia, Universidad Catolica del Norte, Av. Angamos 0610 Antofagasta Chile*
[4] *NAOC, Chinese Academy of Sciences, 20A Datun Rd., Chaoyang District, 100012, Beijing, China*
[5] *Departamento de Astronomia, Universidad de Chile, Camino El Observatorio 1515, Las Condes, Santiago, Chile*

arXiv:1605.03408v1 [astro-ph.SR] 11 May 2016

Accepted –. Received –; in original form –

ABSTRACT

We present the abundance analysis for a sample of 18 red giant branch stars in the metal-poor globular cluster NGC 4147 based on medium and high resolution spectra. This is the first extensive spectroscopic study of this cluster. We derive abundances of C, N, O, Na, Mg, Al, Si, Ca, Ti, Cr, Fe, Ni, Y, Ba, and Eu. We find a metallicity of [Fe/H]=-1.84±0.02 and an α-enhancement of +0.38±0.05 (errors on the mean), typical of halo globular clusters in this metallicity regime. A significant spread is observed in the abundances of light elements C, N, O, Na, and Al. In particular we found a Na-O anti-correlation and Na-Al correlation. The cluster contains only ∼15% of stars that belong to the first generation (Na-poor and O-rich). This implies that it suffered a severe mass loss during its lifetime. Its [Ca/Fe] and [Ti/Fe] mean values agree better with the Galactic Halo trend than with the trend of extragalactic environments at the cluster metallicity. This possibly suggests that NGC 4147 is a genuine Galactic object at odd with what claimed by some author that proposed the cluster to be member of the Sagittarius dwarf galaxy. A anti-relation between the light *s*-process element Y and Na may also be present.

Key words: Chemical Abundances – Globular Cluster: NGC 4147.

1 INTRODUCTION

Galactic globular clusters (GGCs) are known to host star-to-star variations as far as chemical abundances are concerned. More specifically, Carretta et al. (2009b) showed that all GGCs studied up to now have at least a spread (or anti-correlation) in the content of their light-elements O and Na. The only confirmed exception is Ruprecht 106, where Villanova et al. (2013) found that stars share a homogenous chemical composition. This spread is probably due to the early evolution of each cluster, when a second generation of stars (Na-rich and O-poor) was born from gas polluted by ejecta of evolved stars of the first generation (Na-poor and O-rich). This is the so called multiple-population phenomenon.

Carretta et al. (2009b) showed also that most of the stars currently found in a GC belong to the second generation (∼60÷80%). This is at odds with theory, which says that first generation stars must have been much more numerous than what we observe nowadays in order to produce enough ejecta to form the second (D'Ercole et al. 2008). This contradiction can be partially explained if we assume that ejecta were collected preferentially in the center of the cluster due to the gravitational potential. Because of this the second generation was formed in the center and was much less affected by the violent relaxation and the gas expulsion phase during the proto-cluster period (Khalaj & Baumgardt 2015) or by Galactic tidal disruption than the first, which lost most of its members (Caloi & D'Antona 2011).

On the other hand Caloi & D'Antona (2011) suggested the possibility of the existence of clusters that retained almost all the first generation and so only a small fraction of the stars would belong to the second. An example of such a cluster is Terzan 8, where Carretta et al. (2014) found that almost all stars belong to the first generation.

Here we present an opposite case, the Globular Cluster (GC) NGC 4147. This object has an Horizontal Branch (HB) that is mainly populated in the blue part. However it shows also the presence of a red tail. According to Caloi & D'Antona (2011), this indicates that almost all its stars should belong to the second generation, with a fraction of first generation objects that should be very small, probably smaller than all the other GGCs studied up to now. In order to verify this statement we obtained spectro-

⋆ E-mail: svillanova@astro-udec.cl (SV)

scopic data in the Red Giant Branch (RGB) region with the aim of measuring their light-element content. We take advantage of these data also to perform a full chemical analysis of the cluster both to study the chemical trend of its multiple-populations and to compare it with different environments. This is because NGC 4147, based on the projection on the sky of the theoretical orbit of the Sagittarius dwarf spheroidal galaxy computed by Ibata & Lewis (1998), was suggested to be a possible former member of the galaxy (Bellazzini et al. 2003a), like NGC 5053 and NGC 5634, recently studied by Sbordone et al. (2015). Bellazzini et al. (2003b) also found evidence for the presence of Sgr tidal stream stars in the background of NGC 4147 using 2MASS data.

Law & Majewski (2010), on the other hand, used the spatial and kinematic data available for stars associated to the Sgr tidal stream to construct numerical model of the tidal disruption of the galaxy. These authors considered the association of NGC 4147 to Sgr as still possible, but with a low statistical confidence.

In section 2 we describe data reduction and in section 3 the methodology we used to obtain the chemical abundances. In section 4 we present our results including a comparison with different environments (Galactic and extragalactic). Finally in section 5 we give a summary of our findings.

2 OBSERVATIONS, DATA REDUCTION, AND ABUNDANCE ANALYSIS

Our dataset consists of medium and high resolution spectra collected at the GIRAFFE (mounted at the VLT-UT2 telescope) and MIKE (mounted at the Magellan-Clay telescope) spectrograph respectively [1]. Targets were selected from the Stetson et al. (2005) photometry. Three targets were in common between the two datasets.

We observed with GIRAFFE a total of 17 RGB stars with magnitude between V=15.6 and V=18.0. We used the set-up HR12, that gives a spectral coverage between 5820 and 6140 Å with a resolution of R=18700. The signal-to-noise (S/N) is between 25 and 70 at 6000 Å. Data were reduced using the dedicated pipeline (see http://www.eso.org/sci/software/pipelines/). Data reduction includes bias subtraction, flat-field correction, wavelength calibration, sky subtraction, and spectral rectification.

MIKE was used to observe 6 RGB stars with V magnitude between 14.7 and 15.6. The spectrograph cover a wide spectral range, from the ultraviolet to the near infrared, with a resolution of R=32000 (using a slit of 0.7 arcsec). The S/N of the spectra is between 70 and 90 at 6000 Å. Data were reduced using IRAF [2], including bias subtraction, flat-field correction, wavelength calibration, scattered-light and sky subtraction, and spectral rectification.

Radial velocities were measured by the *fxcor* package in IRAF, using a synthetic spectrum as a template. Stars with very different radial velocity with respect to the median value were rejected as non-member. We rejected also two GIRAFFE targets with a radial velocity similar to that of the cluster but with higher metallicities ([Fe/H]$\sim$-1.60). These two stars have low S/N and we could use only one out of the three iron lines available to measure [Fe/H] (see next section). So the disagreement in metallicity is probably due to the combination of the two factors. We end up with a sample of 12 GIRAFFE and 6 MIKE targets. The mean radial velocity we obtained is 179.9$\pm$0.5 km/s. Peterson et al. (1986) and Pryor et al. (1988) give 183.5$\pm$1.3 and 183.2$\pm$0.9 instead. However the first is based on one star only, while the second does not give any detail on the radial velocity measurements they perform so we cannot suggest any reason for this discrepancy. If we compare the mean radial velocity obtained with the two instruments, we get 179.4$\pm$0.5 for GIRAFFE, and 180.7$\pm$1.0 for MIKE (errors on the mean). The two values well agree within 1σ. Table 1 lists the basic parameters of the retained stars: ID (from Stetson et al. 2005), J2000.0 coordinates (RA & DEC in degrees), B and V magnitudes, heliocentric radial velocity RV_H (km/s), T_{eff} (K), log(g), micro-turbulence velocity v_t (km/s), plus [Fe/H], [Na/Fe], [Ca/Fe], and [Ba/Fe] abundances. The determination of the atmospheric parameters and abundances is discussed in the next section. In Fig. 1 we report, on the top of the cluster color magnitude diagram (CMD), the MIKE targets as black filled squares, and with open black circles the GIRAFFE targets.

3 ABUNDANCE ANALYSIS

Atmospheric parameters were obtained in the following way. First, T_{eff} was derived from the B-V color using the relation of Ramirez & Melendez (2005). The reddening we adopted (E(B-V)=0.02) was obtained from Harris (1996, 2010 edition). Surface gravities (log(g)) were obtained from the canonical equation:

$$\log\left(\frac{g}{g_\odot}\right) = \log\left(\frac{M}{M_\odot}\right) + 4\log\left(\frac{T_{\rm eff}}{T_\odot}\right) - \log\left(\frac{L}{L_\odot}\right).$$

where the mass $M/M_\odot$ was assumed to be 0.8 $M_\odot$, and the luminosity $L/L_\odot$ was obtained from the absolute magnitude M_V assuming an apparent distance modulus of $(m\text{-}M)_V$=16.49 (Harris 1996). The bolometric correction (BC) was derived by adopting the relation BC-T_{eff} from Alonso et al. (1999). Finally, micro-turbulence velocity (v_t) was obtained from the relation of Marino et al. (2008).
Atmospheric models were calculated using ATLAS9 (Kurucz 1970) assuming our estimations of T_{eff}, log(g), and v_t, and the [Fe/H] value from Harris (1996)([Fe/H]=-1.80).
The Local Thermodynamic Equilibrium (LTE) program MOOG (Sneden 1973) was used for the abundance analysis. For MIKE data, T_{eff}, log(g), and v_t were re-adjusted and new atmospheric models calculated in an interactive way in order to remove trends in excitation potential and EQW versus abundance for T_{eff} and v_t, respectively, and to satisfy the ionization equilibrium for log(g). 30$\div$40 FeI and

[1] Observations were taken with ESO telescopes at the La Silla-Paranal Observatory under programme ID 083.D-0530, and with LCO telescopes at the Magellan observatory under programme ID CN2011B-039.

[2] IRAF is distributed by the National Optical Astronomy Observatory, which is operated by the Association of Universities for Research in Astronomy, Inc., under cooperative agreement with the National Science Foundation.

Table 1. Parameters for the observed stars including FeI, NaI, CaI and BaII abundances. Reported errors are errors on the mean.

ID	RA	DEC	B	V	RV_H	T_{eff}	log(g)	v_t	[Fe/H]	[Na/Fe]	$[Na/Fe]_{NLTE}$	[Ca/Fe]	[Ba/Fe]
						GIRAFFE							
D1	182.55908	18.53358	17.641	16.845	180.2	4910	2.17	1.38	-1.77	0.48	0.47	0.28	-0.22
D8	182.53150	18.51826	16.128	15.086	178.0	4480	1.23	1.62	-1.81	0.39	0.52	0.44	-0.23
S268	182.50658	18.52611	17.355	16.542	180.3	4840	2.02	1.42	-1.80	0.47	0.48	0.25	-0.41
S377	182.47029	18.55802	17.506	16.725	177.9	4880	2.11	1.39	-1.86	0.73	0.73	0.55	-0.04
S408	182.50379	18.55402	17.496	16.701	177.3	4880	2.10	1.40	-1.81	0.54	0.54	0.29	-0.31
S414	182.50837	18.53466	17.642	16.849	180.2	4910	2.18	1.38	-1.80	0.56	0.55	0.51	-0.34
S429	182.51487	18.53925	16.830	15.950	178.7	4710	1.71	1.49	-1.90	0.70	0.75	0.59	-
S432	182.51587	18.56322	16.756	15.777	178.7	4670	1.62	1.52	-1.86	0.60	0.67	0.52	-0.20
S445	182.51976	18.55226	16.267	15.296	181.0	4540	1.35	1.59	-1.75	0.39	0.50	0.30	-0.23
S688	182.53112	18.53497	16.619	15.688	182.1	4640	1.57	1.53	-1.82	0.49	0.57	0.34	0.03
S690	182.53459	18.53544	16.556	15.629	177.6	4630	1.54	1.54	-1.71	0.51	0.59	0.33	-0.31
S692	182.53587	18.54886	17.532	16.737	181.3	4880	2.12	1.39	-1.92	0.61	0.61	0.58	-0.12
Cluster									-1.79	0.48	0.58	0.42	-0.22
Error									0.03	0.05	0.03	0.04	0.04
						MIKE							
D8	182.53150	18.51826	16.128	15.086	178.9	4430	0.80	1.70	-1.84	0.56	0.46	0.38	-0.19
S437	182.51697	18.54816	15.885	14.716	184.0	4300	0.45	1.80	-1.88	-0.03	-0.11	0.39	-0.22
S445	182.51976	18.55226	16.267	15.296	181.9	4460	0.75	1.59	-1.86	0.69	0.59	0.35	-0.17
S454	182.52253	18.54305	16.257	15.266	177.8	4470	0.85	1.67	-1.84	0.47	0.36	0.45	-0.15
S468	182.52524	18.54625	15.791	14.702	182.6	4300	0.22	1.79	-1.91	0.18	0.10	0.37	-0.04
S690	182.53459	18.53544	16.556	15.629	179.2	4570	1.14	1.53	-1.82	0.71	0.57	-	-0.05
Cluster									-1.86	0.43	0.33	0.39	-0.14
Error									0.01	0.12	0.11	0.02	0.03
Δ(GIR-MIK)	-	-	-	-	-	+63	+0.48	-0.03	+0.08	-	-	+0.00	-0.12

Table 2. Chemical abundances of MIKE stars. The abundance for Ti is the mean of those obtained from the neutral and singly ionized species. Reported errors are errors on the mean.

ID	[CI/Fe]	[NI/Fe]	[OI/Fe]	[CNO/Fe]	[MgI/Fe]	[AlI/Fe]	[SiI/Fe]	[TiI/Fe]	[CrI/Fe]	[NiI/Fe]	[YII/Fe]	[EuII/Fe]
D8	-0.72	0.86	-0.13	0.07	0.38	0.95	0.44	0.30	-0.16	0.03	-0.22	0.45
S437	-0.24	0.21	0.30	0.21	0.47	0.25	0.47	0.31	-0.11	-0.06	-0.01	0.38
S445	-0.64	0.75	-0.27	-0.04	0.38	1.03	0.44	0.25	-0.18	-0.08	-0.33	0.33
S454	-0.26	0.60	0.17	0.17	0.50	0.91	-	0.33	-0.23	-0.07	-0.35	0.37
S468	-0.53	0.54	0.26	0.20	0.46	0.27	0.49	0.27	-0.14	-0.07	-0.11	0.27
S690	-0.61	0.80	0.06	0.14	0.34	1.01	-	0.25	-	-0.05	-0.43	0.42
Cluster	-0.50	0.63	0.07	0.12	0.42	0.74	0.46	0.28	-0.16	-0.05	-0.24	0.37
Error	0.08	0.10	0.09	0.04	0.03	0.15	0.01	0.01	0.02	0.02	0.06	0.03

8÷10 FeII (depending on the S/N of the spectrum) were used for the latter purpose. The [Fe/H] value of the model was changed at each iteration according to the output of the abundance analysis.

For GIRAFFE data we measured Fe, Na, Ca and Ba abundances. Fe abundances were obtained from the equivalent width of the three iron lines at 5914, 5930, and 6065 Å, while for Na we compared the strength of the NaD doublet at 589 nm with suitable synthetic spectra calculated for five different abundances. Finally Ca and Ba abundances were obtained from the lines at 5857, 6102, and 5853 respectively using spectrosynthesis. MIKE data allowed us to perform a more complete abundance analysis and we present here our measurements for C, N, O, Na, Mg, Al, Si, Ti, Cr, Fe, Ni, Y, Ba, and Eu. The line-list and the methodology we used are the same used in previous papers (e.g. Villanova et al. 2013), so we refer to those articles for a detailed discussion about this point. Here we just underline that we took hyperfine splitting into account for Ba. Na abundances were corrected for NLTE using the corrections provided by the INSPEC [3] database. After the NLTE correction, we found a small offset of 0.24 dex between Na abundances of the two datasets, that we could estimate using the 3 stars in common (#S445, #S690, #D8). This is very likely due to some systematic error in the abundance determination of the NaD doublet. This feature is saturated and then its abundance very sensitive to any error in the flat-field or continuum normalization. In order to remove it, we applied a correction of +0.24 dex to GIRAFFE NaD measurements. Abundances for each target are reported in Tables 1 and 2, together with the mean values and the error on the mean.

A detailed internal error analysis was performed by

[3] version 1.0 (http://inspect.coolstars19.com/index.php?n=Main.HomePage)

Table 3. Estimated errors on abundances due to errors on atmospheric parameters and to spectral noise compared with the observed errors for stars #D8. The last column gives the observed dispersion of MIKE data.

ID	ΔT_{eff}=50 K	Δlog(g)=0.10	Δv_t=0.05 km/s	Δ[Fe/H]=0.05	S/N	σ_{tot}	σ_{obs}
Δ([C/Fe])	0.02	0.02	0.05	0.04	0.02	0.07	0.20±0.06
Δ([N/Fe])	0.05	0.02	0.05	0.03	0.02	0.08	0.23±0.07
Δ([O/Fe])	0.05	0.06	0.05	0.02	0.02	0.10	0.23±0.07
Δ([Na/Fe])	0.02	0.01	0.00	0.01	0.05	0.06	0.30±0.09
Δ([Mg/Fe])	0.03	0.01	0.00	0.01	0.05	0.06	0.06±0.02
Δ([Al/Fe])	0.02	0.00	0.02	0.01	0.05	0.06	0.39±0.11
Δ([Si/Fe])	0.05	0.01	0.02	0.01	0.05	0.07	0.02±0.01
Δ([Ca/Fe])	0.00	0.00	0.00	0.00	0.04	0.04	0.04±0.01
Δ([Ti/Fe])	0.03	0.00	0.00	0.01	0.03	0.04	0.03±0.01
Δ([Cr/Fe])	0.03	0.00	0.00	0.00	0.03	0.04	0.05±0.01
Δ([Fe/H])	0.05	0.01	0.02	0.01	0.01	0.05	0.03±0.01
Δ([Ni/Fe])	0.00	0.00	0.00	0.00	0.02	0.02	0.04±0.01
Δ([Y/Fe])	0.07	0.04	0.03	0.00	0.04	0.09	0.16±0.05
Δ([Ba/Fe])	0.03	0.05	0.03	0.03	0.01	0.07	0.07±0.02
Δ([Eu/Fe])	0.05	0.03	0.03	0.02	0.02	0.07	0.04±0.01

varying T_{eff}, log(g), [Fe/H], and v_t and redetermining abundances of star #D8, assumed to represent the entire MIKE sample. GIRAFFE data will not be used to check for intrinsic spreads, so error analysis is not required for them. We just give in Tab. 1 the mean differences in T_{eff}, log(g), v_t, [Fe/H], [Ca/Fe], and [Ba/Fe] with respect MIKE data based on the three stars in common. Parameters for stars #D8 were varied by ΔT_{eff}=+50 K, Δlog(g)=+0.10, Δ[Fe/H]=+0.05 dex, and Δv_t=+0.05 km/s. This estimation of the internal errors for atmospheric parameters was performed as in Marino et al. (2008). Results are shown in Tab. 3, including the error due to the noise of the spectra. This error was obtained for elements whose abundance was obtained by EQWs, as the errors on the mean given by MOOG, and for elements whose abundance was obtained by spectrum-synthesis, as the error given by the fitting procedure. σ_{tot} is the squared sum of the single errors, while σ_{obs} is the mean observed dispersion of MIKE data.

As a cross check of our abundance analysis, we plot in Fig. 2 and Fig. 3 [Fe/H], [Na/Fe], [Ca/Fe], and [Ba/Fe] vs. T_{eff} for the entire sample. The temperature range covered by our stars is about 600 K. As far as iron, calcium and barium are concern, a linear fit gives a slopes with a significance below 1σ. We plot also the mean abundance for each element and the $\pm1\sigma$ error. Again all stars are spread around the mean value and no sign of trend is present. After this check we conclude that the two different methods we used for GIRAFFE and MIKE targets are consistent over the entire temperature range.

If we move to Na instead, we see a different situation. First of all we considered only stars with temperature hotter than 4400 K. Again a linear fit gives a slopes with a significance below 1σ and all stars are spread around the mean value with no sign of any trend. However the two coldest targets show a Na content much lower than that of their hotter companions. If we extrapolate the fit to the temperature of the two coldest stars, we find a difference with respect to the fit of $\sim$0.50 dex, that is significant at a level of $\sim4\sigma$. This is because they are first generation stars with an intrinsic low Na, while all the other targets are second generation stars with high Na. In order to show visually the large difference in Na content of the two coldest stars with respect to the rest of the sample we plot in Fig. 4 the spectra of the Na-rich #D8 (black squares) and the Na-poor #S437 (red squares) target around the Na double at 568 nm. Blue lines are the best fitting synthetic spectra with Na abundances taken from Tab. 1. The green line is a synthetic spectrum calculated for the atmospheric parameters of #S437 but with the Na content of #D8. It is clear from this comparison that the #S437 strong Na under abundance is real and not due, for instance, to the low S/N or to an ill-estimated stellar effective temperature.

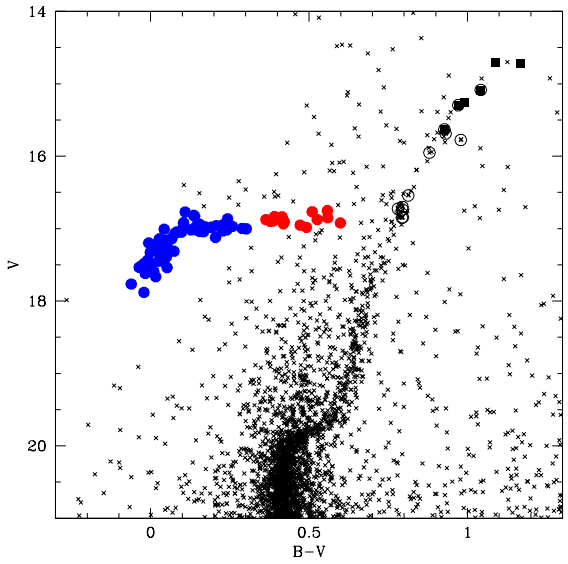

Figure 1. V vs. B-V CMD of NGC 4147. Open black circles indicate GIRAFFE targets, while filled black circles indicate MIKE targets. HB stars were divided in first generation (filled red circles) and second generation (filled blue circles) objects. See text for more details.

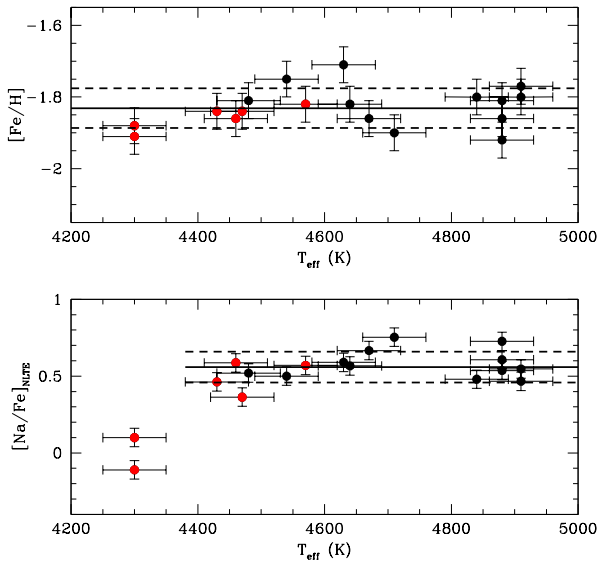

Figure 2. [Fe/H] vs. T_{eff} (upper panel) and [Na/Fe] vs. T_{eff} (lower panel) relations for our sample. GIRAFFE targets are reported as black circles, while MIKE targets are reported as red circles. Error adopted are those from Tab. 3. For both relations we indicated the mean value with a continuous black line and the $\pm 1\sigma$ interval with two dashed lines. For the [Na/Fe] vs. T_{eff} relation we considered only targets hotter than 4400 K. See text for more details.

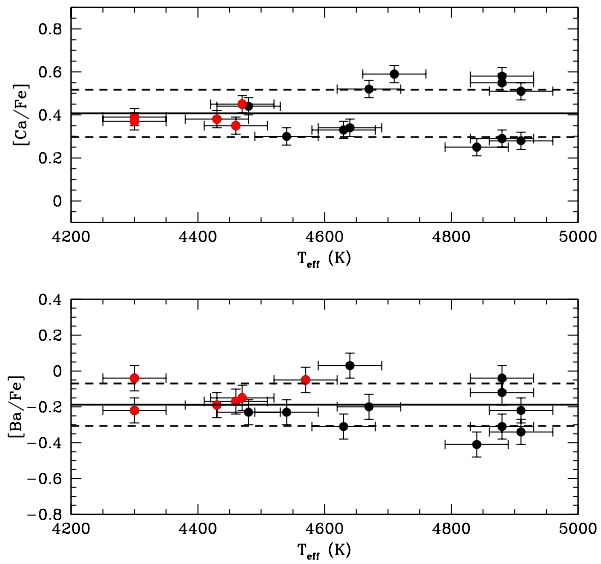

Figure 3. [Ca/Fe] vs. T_{eff} (upper panel) and [Ba/Fe] vs. T_{eff} (lower panel) relations for our sample. GIRAFFE targets are reported as black circles, while MIKE targets are reported as red circles. Error adopted are those from Tab. 3. For both relations we indicated the mean value with a continuous black line and the $\pm 1\sigma$ interval with two dashed lines.

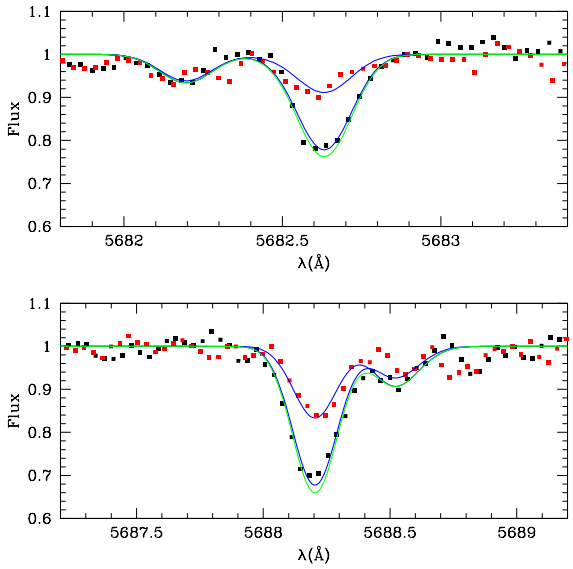

Figure 4. Spectra of the #D8 (black squares) and #S437 (red squares) targets around the Na double at 568 nm. Blue lines are the best fitting synthetic spectra with Na abundances taken from Tab. 1. The green line is a synthetic spectrum calculated for the atmospheric parameters of #S437 but with the Na content of #D8.

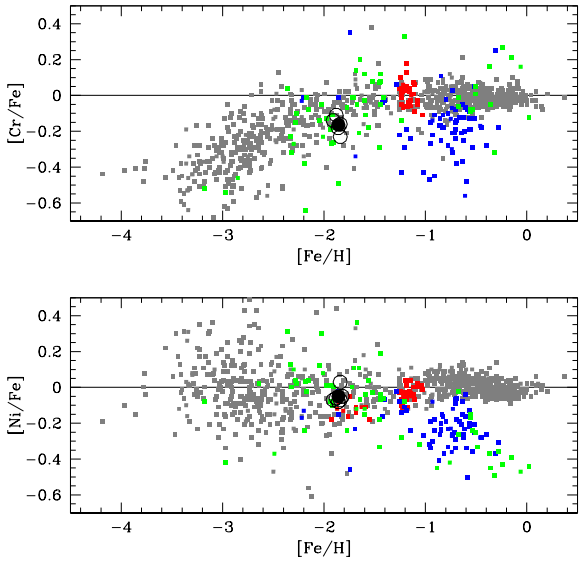

Figure 5. [Cr/Fe] and [Ni/Fe] trends as a function of [Fe/H] for different environments (see text). Open black circles indicate MIKE targets, while the filled black circle is the mean abundance of NGC 4147.

4 RESULTS

4.1 Iron-peak elements

The iron content we obtained from GIRAFFE data is:

$$[Fe/H]_{GIRAFFE} = -1.82 \pm 0.02$$

while from MIKE data is:

$$[Fe/H]_{MIKE} = -1.86 \pm 0.01$$

Reported errors are errors on the mean. The difference between the two datasets is of 0.04 dex, that correspond to 1.8 σ. The agreement is satisfactory. Finally we can give a value for the iron content of the cluster that is the mean of the two datasets:

$$[Fe/H] = -1.84 \pm 0.02$$

This value well agrees with Ivans I.I. (2009), that give [Fe/H]=-1.7±0.1, and with Harris (1996) that give [Fe/H]=-1.80. The measured iron dispersion in Tab. 3 well agrees with the dispersion due to measurement errors so we can rule out any intrinsic Fe abundance spread.

The chemical abundances for the iron-peak elements Cr and Ni are listed in Table 2. The value is sub-solar for Cr, while Ni is basically solar-scaled. Figure 5 (as well as the following plots) shows the mean (black filled circle) and star by star (black empty circles) elemental abundances of the cluster compared with a variety of galactic and extra-galactic objects. We have included values from GGCs (Carretta et al. 2009b; Villanova et al. 2010, 2011, red filled squares); Disc and Halo stars (Fulbright 2000; Reddy et al. 2003, 2006; Cayrel et al. 2004; Simmerer 2004; Barklem et al. 2005; Francois et al. 2007, gray filled squares) and extra-galactic objects such as Magellanic clouds (Pompeia et al. 2008; Johnson et al. 2006; Mucciarelli et al. 2008, 2009, blue filled squares), Draco, Sextans, Ursa Minor and Sagittarius dwarf galaxy and the ultra-faint dwarf spheroidals Boötes I and Hercules (Monaco et al. 2005; Sbordone et al. 2007; Shetrone et al. 2001; Ishigaki et al. 2014; Koch et al. 2008, green filled squares).

Around NGC 4147 metallicity, Galactic and extragalactic environments share the same iron-peak abundances, with only very few extragalactic stars showing a Cr depletion. NGC 4147 iron-peak elements agree with both environments and do not support or disproof an extragalactic origin of this object.

4.2 Light elements

Light elements C, N, O, Na and Al have an observed spread that well exceeds the observational uncertainties (see Tab. 3). The only exception is Mg that seems to be homogeneous within the errors.

Very interesting is the analysis of the Na and O distributions. In Fig. 6 we show the Na-O anticorrelation of MIKE data on the left panel, while in the right panel we report the Na distribution based on the GIRAFFE and MIKE data. We fitted the Carretta et al. (2009a) diluition model (blue line) to the Na-O anticorrelation. According to this fit the cluster is composed by a first generation of stars with [Na/Fe]∼+0.0 and [O/Fe]∼+0.3 and second generation with [Na/Fe]∼+0.5 and [O/Fe]∼-0.2. This is in common with all but one of the globular clusters studied up to now. The difference appears when we count the number of stars for each population. If we combine together the two datasets and consider all the stars with [Na/Fe]<0.30 as first generation, we end up with

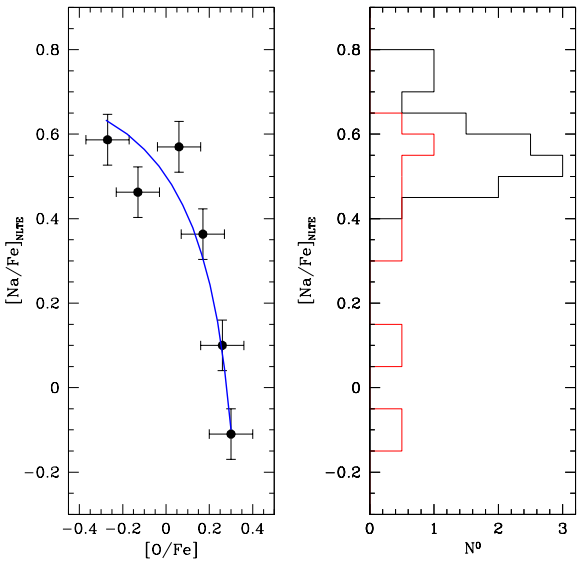

Figure 6. Left panel: [Na/Fe] vs. [O/Fe] as obtained for MIKE targets. The cluster shows the typical Na-O anti-correlation of GGCs. The blue line is the Carretta et al. (2009a) diluition model for the cluster. Right panel: The Na distribution of GIRAFFE (black) and MIKE (red) targets. See text for more details.

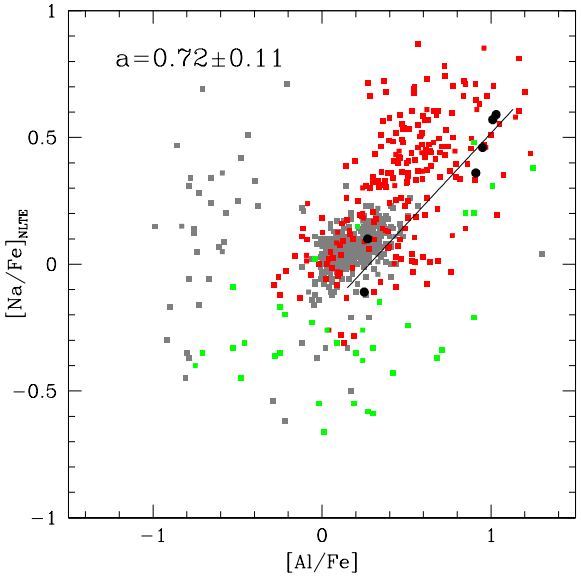

Figure 7. [Na/Fe] vs. [Al/Fe] as obtained for MIKE targets (filled black circles). The cluster shows the typical Na-Al correlation of GGCs (red squares). See text for more details.

the result that that second generation stars in the cluster represent ∼90 % of the total, leaving room only for a ∼10 % to the first generation. The poissonian error related with the two estimations is 20 and 10 % respectively. This result is confirmed by Fig. 1. Here we selected tentatively the HB progeny of the first generation as red filled circles, and the HB progeny of the second generation as blue filled circles. If we compare the relative number of stars, we obtain

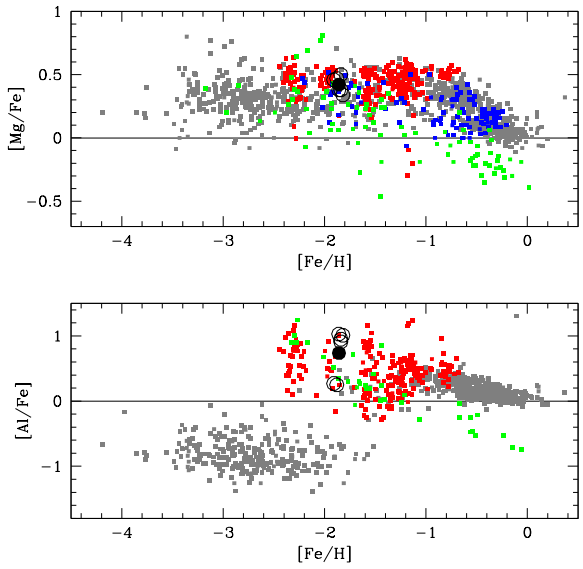

Figure 8. [Mg/Fe] and [Al/Fe] trends as a function of [Fe/H] for different environments (see text). Open black circles indicate MIKE targets, while the filled black circle is the mean abundance of NGC 4147.

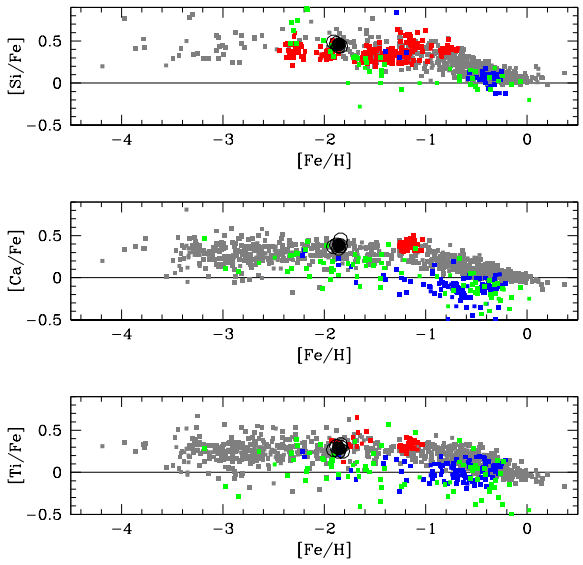

Figure 9. [Si/Fe], [Ca/Fe] and [Ti/Fe] trends as a function of [Fe/H] for different environments (see text). Open black circles indicate MIKE targets, while the filled black circle is the mean abundance of NGC 4147.

that second generation stars in the cluster represent 80±10 % of the total. However we point out that this number is a lower limits because we left out blue HB stars evolved off the blue HB zero age sequence, and at the same time red HB stars suffer a contamination from the field. So our best estimation is that ∼85 % of the stars in NGC 4147 belong to the second generation. If Caloi & D'Antona (2011) or Khalaj & Baumgardt (2015) are right, we have here a cluster that suffered an extreme loss of its first generation.

In Fig. 7 we show the correlation between Na and Al, another elements usually but not always involved in the light-element spread (Villanova et al. 2011). The cluster shows a clear correlation that matches that found in the other GGCs. In addition the two first generation stars ([Na/Fe]∼0.0, [Al/Fe]∼0.2) well agrees with the bulk of Galactic objects while very few extragalactics targets occupy this region. In the Figure we report also the slope and its error. The significance of the relation of of ∼7σ.

Finally in Fig. 8 we show the Mg and Al vs. Fe trends. NGC 4147 nicely follow the galactic and extragalactic trend as far as Mg is concern. Al shows a more surprising behavior. If we consider only Milky Way stars, they follow two separate trends. Almost all stars above [Fe/H]∼-1.7 have [Al/Fe]⩾0, while all stars below [Fe/H]∼-1.7 have [Al/Fe] well below 0 with a mean value of ∼-0.8. This result is not totally new, because Gehren et al. (2006, Fig. 5) found the same behavior using [Al/Mg] vs. [Fe/H] instead of [Al/Fe] vs. [Fe/H] as we do. The surprise arrises when we add GGC and extragalactic dwarfs because in both classes of objects stars below [Fe/H]∼-1.7 have [Al/Fe]⩾0. This could suggest a different formation history of GCC stars with respect the Halo field. In any case NGC 4147 follow the GCC trend.

4.3 α elements

The α elements Si, Ca, and Ti are overabundant compared to the Sun. This is a common feature among almost every GGC as well as among similarly metal-poor field stars in the Milky Way and in outer galaxies. The calcium content we obtained from GIRAFFE data is:

$$[Ca/Fe]_{GIRAFFE} = +0.42 \pm 0.04$$

while from MIKE data is:

$$[Ca/Fe]_{MIKE} = +0.39 \pm 0.02$$

Reported errors are errors on the mean. The difference between the two datasets is of 0.03 dex, within 1σ. The agreement is satisfactory. Based on Mg, Si, Ca, and Ti abundances of MIKE stars, we derive for the cluster a mean α element abundance of:

$$[\alpha/Fe] = +0.39 \pm 0.04$$

Figure 9 shows the α-element abundance of the cluster (MIKE data only), compared with the trend as a function of the metallicity for GGCs, disk and halo stars and extragalactic objects. The α elements in NGC 4147 follows the same trend as GGCs and are fully compatible with Halo field stars. Again NGC 4147 falls in a region where both Galactic and extragalactic objects overlap. However if we look carefully at the Ca trend, we notice that at the metallicity of the cluster the mean Ca abundance for Halo stars is higher than that for dwarf galaxies. The difference is of ∼0.3 dex. This is true also for Ti. NGC 4147 stars have:

$$[Ca/Fe] = +0.40 \pm 0.02$$

and

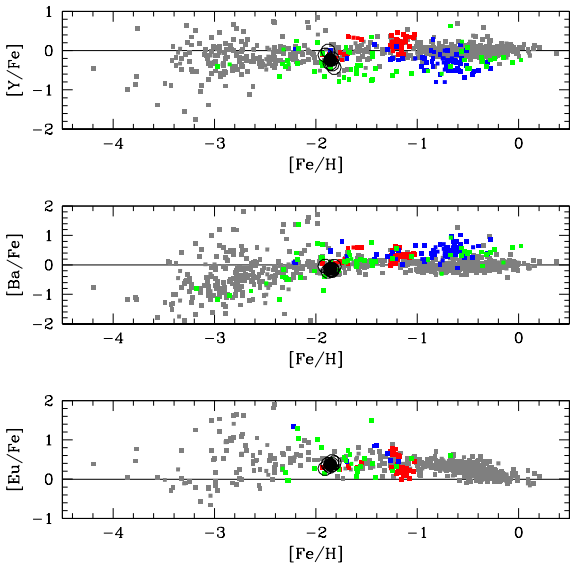

Figure 10. [Y/Fe], [Ba/Fe] and [Eu/Fe] trends as a function of [Fe/H] for different environments (see text). Open black circles indicate MIKE targets, while the filled black circle is the mean abundance of NGC 4147.

$$[Ti/Fe] = +0.28 \pm 0.02$$

(reported errors are errors on the mean) that must be compared with the mean values for the Halo ($[Ca/Fe] \sim 0.3$, $[Ti/Fe] \sim 0.3$) and for the Dwarf galaxies ($[Ca/Fe] \sim 0.1$, $[Ti/Fe] \sim 0.1$). So, according the its α-element content, NGC 4147 seems more likely to be a genuine Galactic cluster, although some other clusters like M54 and Arp2, that belong to the Sagittarius galaxy, have a α-element content similar to NGC 4147 ([Ca/Fe]=+0.32 and [Ca/Fe]=+0.46 respectively,Carretta et al. 2010; Mottini et al. 2008).

4.4 Heavy Elements

While light-element variations are well-known in GCs, intrinsic dispersion among heavier elements is less common. Most of the heavier elements (Z > 30) are produced either by slow or rapid neutron-capture reactions (the so-called s and r processes). s-process happens in a different physical condition with respect to r-process and are thus likely to happen in different astrophysical sites. We measured the abundances of the neutron-capture elements: Y, Ba, and Eu. Y and Ba are mainly produced by the s-process at solar metallicity, while Eu is produced almost exclusively in the r-process. The mean Y and Ba abundance ratios are slightly sub-solar, while Eu is heavily super-solar. Figure 10 shows the mean heavy-element ratios of the cluster (MIKE data only), compared with the trend as a function of the metallicity of GGCs, disk and halo stars and extragalactic objects. All three elements agree with Milky Way Halo as well as with extragalactic environment. Figure 11 shows the mean [Ba/Y] and [Eu/Y] ratios, where again NGC 4147 agrees both with the Galactic and the extragalactic trends

Ba and Eu show an observed spread that is comparable to that expected from the errors (see Table 3), while for Y the observed spread is significantly larger. To check this behavior, we show in Figure 12 the abundance ratios of [Y/Fe] as a function of [Na/Fe]. The two first generation stars ([Na/Fe]∼0.0) well agrees with the bulk of Galactic objects while most of the extragalactic stars have lower Na and Y content. This support our identification of NGC 4147 as a Galactic cluster. What is more interesting is the anticorrelation between Y and Na with Y that decreases while Na increases. In the plot we reported the slope a of the linear fit to NGC 4147 stars (black line) together with its error. The significance of the fit is larger than 4σ.

Only a handful of metal-poor globular clusters show a potential star-to-star dispersion in neutron-capture elements (Kacharov et al. 2013; Worley et al. 2013). Marino et al. (2009) found a wide range of abundances values for s-process elements, Y, Zr and Ba, in M22. They also identified a bimodality among these elements. However none of the elements show a correlation with Na, O and Al.

Our result implies that the second Na-rich generation was formed by material where Y was destroyed. This is at odd with current models that describe the multiple population phenomenon in GCs, which postulate AGB stars as major polluters (Ventura et al. 2009). In fact AGB stars also produce light s-process elements like Y (Cristallo et al. 2015). The amount of light s-element produced depends a lot on the mass of the AGB star, but in no case a Y destruction is predicted. For this reason we checked for possible blending not considered in our line-list. For example a blend with a CN or CH line could mimic a [Y/Fe] spread even if Y is constant just because C and N vary. However the result of this check was negative. We underline also that the fact that the two Y-rith first genaration stars are also the two coldest objects in our sample. We have no first generation stars in the temperature range of the second generation targets, so we cannot totally roule out a possible temperature effect on our Y abundance determination. In spite of that we leave open the possibility that the [Y/Fe] vs. [Na/Fe] trend we found is real waiting for future studies.

5 SUMMARY

In this paper we present the first detailed chemical abundances of 15 elements in 6 red giant radial velocity members of NGC 4147 observed using the high resolution MIKE spectrograph, mounted at the Magellan-Clay telescope, and Fe and Na abundances in 12 red giant radial velocity members observed using the medium resolution GIRAFFE spectrograph, installed at the VLT-UT2 telescope. Chemical abundances have been computed using plane-parallel atmospheric-models and LTE approximation. Equivalent width method has been used when possible. Otherwise we applied the spectrum-synthesis method. We obtained the following results:

- We found a mean metallicity of [Fe/H]=-1.84±0.02, that well agree with previous literature data. As far as other iron-peak elements are concerned, Cr is sub-solar while Ni is solar-scaled, in agreement with Halo and dwarf galaxies environment at the cluster metallicity
- NGC 4147 shows the typical Na-O anticorrelation common to almost all the other GGCs. However the cluster contains only ∼15% of first generation stars. This implies that it suffered a severe mass loss, maybe the most extreme among

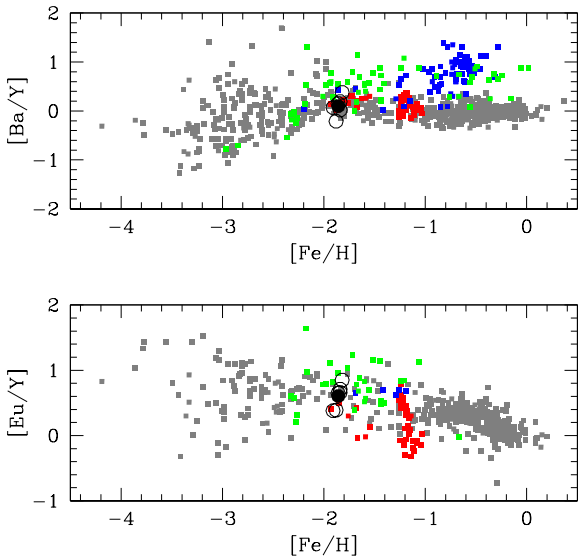

Figure 11. [Ba/Y] and [Eu/Y] trends as a function of [Fe/H] for different environments (see text). Open black circles indicate MIKE targets, while the filled black circle is the mean abundance of NGC 4147.

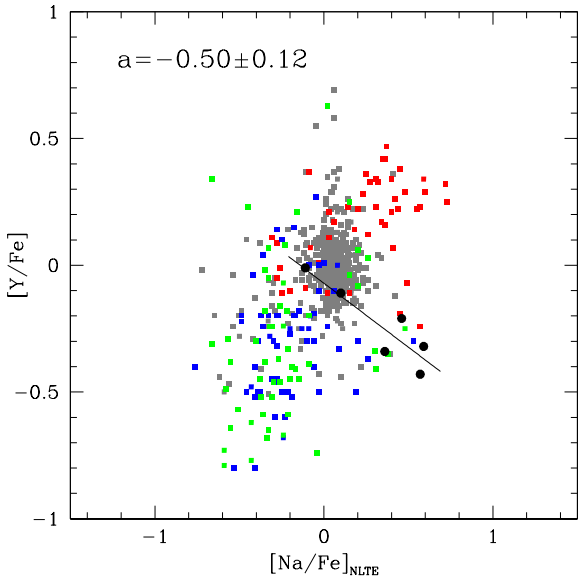

Figure 12. [Y/Fe] vs. [Na/Fe] as obtained for MIKE targets (filled black circles). The cluster shows a possible Y-Na anti-correlation. See text for more details.

all the GGCs. Na is also correlated with Al as found in many GGCs. Mg follows the Galactic trend, while Al is much more enhanced with respect to Halo stars sharing this behaviors with all the other GGCs.

- NGC 4147 has the typical α-enhancement of the Halo. Its Ca and Ti abundances agree better with the Halo than with the mean Ca and Ti content of extragalactic environments at the cluster metallicity. This is true also if we consider the behavior of [Na/Fe] vs. [Al/Fe] and [Y/Fe] vs. [Na/Fe].
- Heavy elements Y, Ba and Eu have mean abundances that match those of the Milky Way and of extragalactic environments. While Ba and Eu are homogeneous, Y possibly shows a spread and an anticorrelation with Na.

ACKNOWLEDGMENTS

SV and CMB acknowledge the support provided by Fondecyt Regular 1130721 and 1150060, respectively. PA acknowledges the support provided by the Chinese Accademy of Sciences President's International Fellowship Initiative, Grant N. 2014FFJB0018, and by the Programa de Astronomia, Fondo China-Conicyt 2Conv. CAS15020.

REFERENCES

Alonso, A., Arribas, S., & Martinez-Roger, C. 1999, A&AS, 140, 261
Barklem, P. S., Christlieb, N., Beers, T. C., Hill, V., Bessell, M. S., Holmberg, J., Marsteller, B., Rossi, S., Zickgraf, F. J., & Reimers, D. 2005, A&A, 439, 129
Bellazzini, M., Ferraro, F. R., & Ibata, R. 2003(a), AJ, 125, 188
Bellazzini, M., Ibata, R., Ferraro, F. R., & Testa, V. 2003(b), A&A, 405, 577
Caloi, V., & D'Antona, F. 2011, MNRAS, 417, 228
Carretta, E., Bragaglia, A., Gratton, R.G., Lucatello, S., Catanzaro, G., Leone, F., Bellazzini, M., Claudi, R., D'Orazi, V., Momany, Y., Ortolani, S., Pancino, E., Piotto, G., Recio-Blanco, A., & Sabbi, E. 2009, A&A, 505, 117
Carretta, E., Bragaglia, A., Gratton, R.G., Lucatello, S., Catanzaro, G., Leone, F., Bellazzini, M., Claudi, R., D'Orazi, V., & Momany, Y. 2009, A&A, 505, 139
Carretta, E., Bragaglia, A., Gratton, R. G., Lucatello, S., Bellazzini, M., Catanzaro, G., Leone, F., Momany, Y., Piotto, G. & D'Orazi, V. 2010, A&A, 520, 95
Carretta, E., Bragaglia, A., Gratton, R. G., D'Orazi, V., Lucatello, S. & Sollima, A. 2014, A&A, 561, 87
Cayrel, R., Depagne, E., Spite, M., Hill, V., Spite, F., Francois, P., Plez, B., Beers, T., Primas, F., Andersen, J. et al. 2004, A&A, 416, 1117
Cristallo, S., Straniero, O., Piersanti, L., & Gobrecht, D. 2015, ApJS, 219, 40
D'Ercole, A., Vesperini, E., D'Antona, F., McMillan, S.L.W., & Recchi, S. 2008, MNRAS, 391, 825
Fulbright, J. P. 2000, AJ, 120, 1841
Francois, P., Depagne, E., Hill, V., Spite, M., Spite, F., Plez, B., Beers, T. C., Andersen, J., James, G., Barbuy, B. et al. 2007, A&A, 476, 935
Gehren, T., Shi, J.R., Zhang, H.W., Zhao, G., & Korn, A.J. 2006, A&A, 451, 1065
Harris, W.E. 1996, AJ, 112, 1487
Ibata, R. A., Gilmore, G., & Irwin, M. J. 1994, Nature, 370, 194
Ibata, R. A., & Lewis, G. F. 1998, ApJ, 500, 575
Ishigaki, M. N., Aoki, W., Arimoto, N., & Okamoto, S. 2014, A&A, 562, 146
Ivans, I.I. 2009, AAS, 21340716I

Johnson, J. A., Ivans, I. I., & Stetson, P. B. 2006, ApJ, 640, 801
Kacharov, N., Koch, A., & McWilliam, A. 2013, A&A, 554, 81
Khalaj, P. & Baumgardt, H., 2015, MNRAS, 452, 924
Koch, A., McWilliam, A., Grebel, E. K., Zucker, D. B., & Belokurov, V. 2008, ApJ, 688, 13
Kurucz, R.L. 1970, SAO Special Report, 309
Law, D. R., & Majewski, S. R. 2010, ApJ, 718, 1128
Marino, A.F., Villanova, S., Piotto, G., Milone, A.P., Momany, Y., Bedin, L.R. & Medling, A.M. 2008, A&A, 490, 625
Marino, A.F., Milone, A.P., Piotto, G., Villanova, S., Bedin, L.R., Bellini, A., & Renzini, A. 2009, A&A, 505, 1099
Mottini, M., Wallerstein, G., & McWilliam, A. 2008, AJ, 136, 614
Mucciarelli, A., Carretta, E., Origlia, L., & Ferraro, F. R. 2008, AJ, 136, 375
Mucciarelli, A., Origlia, L., Ferraro, F. R.,.& Pancino, E. 2009, ApJ, 695, 134
Monaco, L., Bellazzini, M., Bonifacio, P., Ferraro, F. R., Marconi, G., Pancino, E., Sbordone, L., & Zaggia, S. 2005, A&A, 441, 141
Peterson, R.C., Olszewski, E.W., & Aaronson, M. 1986, ApJ, 307, 139
Pompeia, L., Hill, V., Spite, M., Cole, A., Primas, F., Romaniello, M., Pasquini, L., Cioni, M.R., & Smecker Hane, T. 2008, A&A, 480, 379
Pryor, C., McClure, R.D., Fletcher, J.M., & Hesser, J.E. 1988, IAUS, 26, 661
Ramirez, I., & Melendez, J. 2005, ApJ, 626, 446
Reddy, B. E., Tomkin, J., Lambert, D. L., & Allende Prieto, C. 2003, MNRAS, 340, 304
Reddy, B. E., Lambert, D. L., & Allende Prieto, C. 2006, MNRAS, 367, 1329
Sbordone, L., Bonifacio, P., Buonanno, R., Marconi, G., Monaco, L., Zaggia, S. 2007, A&A, 465, 815
Sbordone, L., Monaco, L., Moni Bidin, C., Bonifacio, P., Villanova, S., Bellazzini, M., Ibata, R., Chiba, M., Geisler, D., Caffau, E., & Duffau, S. 2015, A&A, 579, 104
Shetrone, M. D., Cote, P., Sargent, W. L. W. 2001, ApJ, 548, 592
Simmerer J. 2004, AAS, 205, 7705
Sneden, C. 1973, ApJ, 184, 839
Stetson, P.B., Catelan, M., & Smith, H.A. 2005, PASP, 117, 1325
Ventura, P. & D'Antona, F. 2009, A&A, 499, 835
Villanova, S., Geisler, D., & Piotto, G. 2010, ApJ, 722, 18
Villanova, S., & Geisler, D. 2011, A&A, 535, 31
Villanova, S., Geisler, D., Carraro, G., Moni Bidin, & C., Muoz, 2013, ApJ, 778, 186
Worley, C. C., Hill, V., Sobeck, J., & Carretta, E. 2013, A&A, 553, 47

This paper has been typeset from a TEX/ LATEX file prepared by the author.